Reduction of Iron Oxide in Gas-Conveyed Systems

N. J. THEMELIS and W. H. GAUVIN

McGill University and Pulp and Paper Research Institute of Canada, Montreal, Quebec, Canada

The model particles were prepared by oxidation of carbonyl iron spheres, followed by fractionation into cuts of very narrow size. A two-wavelength radiation pyrometer was developed for measuring the temperature of the particles in flight, and special probes were designed for determining gas velocity and degree of reduction at different levels of the reactor.

The authors have reported elsewhere (*1*) that an analysis based on numerous published data (*2* to *14*) as well as on their own experimental results showed that the reduction of iron oxides takes place at the interface between the reduced and unreduced layers. Physically this implies that while the reducing gas can advance through the interstitial microporosity created by the removal of oxygen atoms from the oxide lattice, it cannot penetrate the dense unreduced crystal.

It was also shown that in the absence of diffusional resistance through the boundary layer the reduction rate is probably controlled by the rate of reaction at the interface, and consequently the rate of advance of the latter towards the center of the particle is constant with time. Under these conditions the following rate equation was derived from experimental hydrogen-reduction data covering a wide range of temperature and particle size (from a few hundred microns up to 5 cm. in nominal diameter), as well as different initial states of oxidation and extents of reduction:

$$[1-(1-R_x)^{1/3}]/\theta = [0.150e^{-E/RT}]/d_p \quad (1)$$

A similar equation was developed for reduction by carbon monoxide, though in this case only a few experimental data were available:

$$[1-(1-R_x)^{1/3}]/\theta = [0.025e^{-E/RT}]/d_p \quad (2)$$

In developing the above equations no distinction was made between different types of oxides and ores and no consideration was given to the effect of the physical properties of the reduced particles. Therefore it would be expected that the experimental scatter from the proposed correlations is due to these variations (*1*).

Considering the complex physical phenomena which accompany reduction, such as cracking, sintering, crystallization, etc., the term *temperature coefficient* should be more appropriate than *activation energy* in denoting the combined effects of temperature on both the physical and chemical phenomena associated with reduction. Regarding the problem of obtaining the value of this coefficient, the most acceptable approach was to neglect variations in E with temperature and estimate an average value applying over the whole temperature range of experimental work in this field. The resulting value of 4,200 cal./g.-mole, which indicated a fivefold increase in reaction rates between 400° to 1,000°C., was deemed to fit best the experimental data available.

When the concentration of water vapor at the reaction interface has an appreciable value c, the corresponding rate equation may be expressed as follows:

$$[1-(1-R_x)^{1/3}]/\theta = [0.150e^{-E/RT}/d_p][(c_e-c)/c_e] \quad (3)$$

The aims of the present work may be summarized as follows:

1. To extend correlation (1) to the lower range of particle sizes, from 5 to 100 μ in diameter.

2. To determine the effect of temperature on the reduction, and, if possible, establish the influence of associated physical phenomena on the rate of the process. The experiments covered the temperature range between 500° and 1,100°C.

3. To study the behavior of iron oxide particles moving with the reducing gas. The standard experimental technique of reducing a stationary particle in a stream of gas could not be used in the present study. Careful consideration of the alternatives led to the adoption of the atomized suspension technique (*15, 16, 17*) as the most convenient method of studying the reduction of small particles.

This process, which has been under development for the past few years, involves the suspension of liquid droplets or fine solid particles in a gaseous stream flowing downward or upward through a vertical reactor tube. The walls of the tube are maintained at a high temperature level by external heating, and the rate of heat transfer to the stream is correspondingly high. This technique was selected for the present study because it afforded excellent contact between the particles and the reducing gas, while providing a very effective means of controlling the particle residence time by changing the gas flow rate or the distance travelled by the particle.

EXPERIMENTAL

Reactor

The reactor consisted of a 4.4-in. I.D. × 8.5 ft. long tube made of 330-stainless steel, ⅜ in. thick, and supported in a vertical position, as shown in Figure 1. The tube was heated by means of Kanthal strips coiled in spirals and embedded in refractory cement which acted as a support to the elements at high temperatures.

N. J. Themelis is with Noranda Research Center, Montreal, Quebec, Canada.

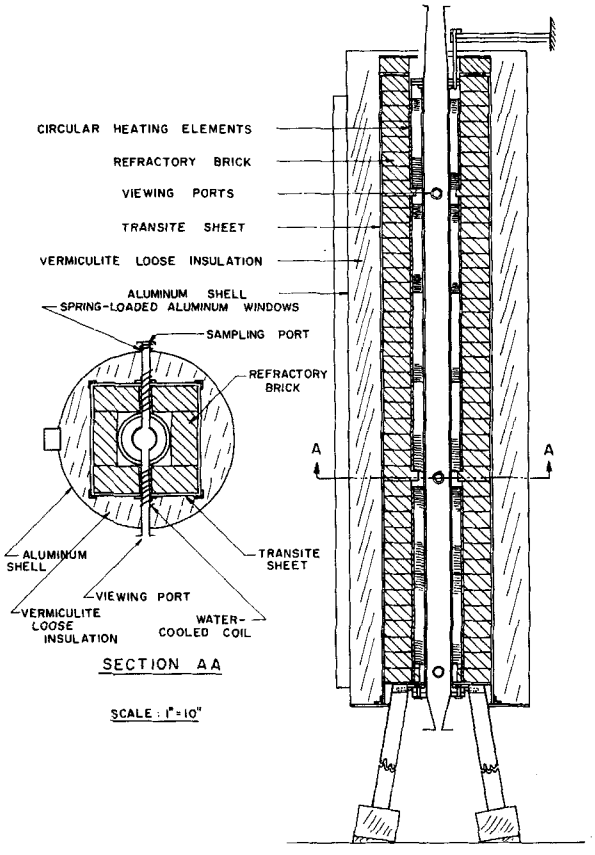

Fig. 1. Atomized suspension technique reactor.

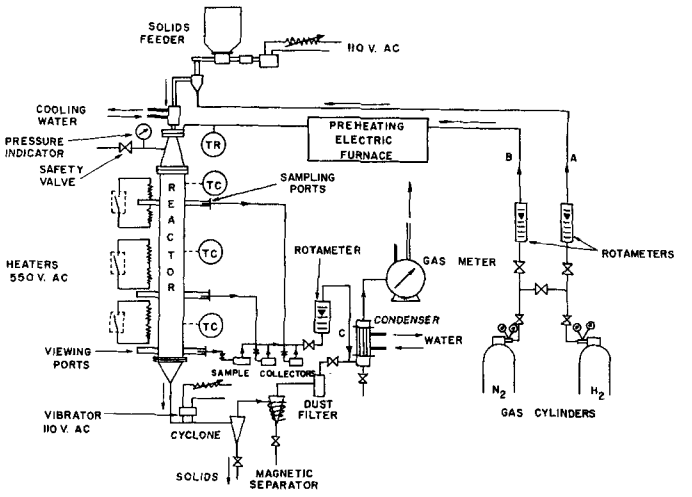

Fig. 2. Flow sheet of apparatus.

The reactor tube was provided with six 1-in. I.D. water-cooled ports arranged in diametrically opposed pairs at three different levels of the tube. The purpose of three of these ports was to allow pyrometric temperature measurements of the particles during reduction, while the others were used for introducing sampling and thermocouple probes into the reactor.

Two special temperature probes were used during the investigation for measuring the temperature of gas streams. The first was a conventional suction thermocouple with double shield. The second probe was used for measuring the temperature of particle-laden gases and consisted of a low-suction thermocouple whose shield was heated electrically. The temperature of the shield was maintained close to that of the gas, thereby minimizing radiation losses from the thermocouple junction to the shield.

A schematic flow diagram of the reactor apparatus is shown in Figure 2. Hydrogen or nitrogen gas from the storage cylinders could be fed into the reactor through the preheating furnace and the solids feeder. For very fine solids it was necessary to disperse the particles before introducing them to the reactor; this was done by means of a spouted-bed cone (*18*) into which solids were fed from the top while a jet of gas was introduced through a nozzle in the bottom. The gas-solid dispersion was then led into the reactor through a side outlet in the cone. The gaseous suspension of oxides flowed downwards through the reactor tube and was then led to the cyclone separators, filter, and gas metering apparatus.

Samples of the reduced oxide could be obtained from the cyclone separator and also through the three sampling ports.

Two Wave Length Radiation Pyrometer

Since the heat of reaction may affect the temperature of a reacting particle considerably, it could not be assumed at the beginning of this investigation that the particle temperature was equal to that of the gas stream or of the reactor walls. To measure this temperature without interfering with the particle flow a pyrometric method was developed based on the two wave length radiation theory which was originally formulated by Schack. The development and design work on this pyrometer have been described elsewhere (*19*). As would be expected from the theoretical consideration the accuracy of the instrument was found to be independent of emissivity and of all geometric factors; the pyrometer could be used both in the infrared and the optical ranges of radiation by interchanging filters and photoelectric cells.

Preparation of Model Oxide Spheres

To facilitate the mathematical analysis of the reduction data it was highly desirable to work with particles of uniform size and shape. However all technical and reagent grades of iron oxides are only available in the form of very small particles (0.1 to 3μ) which cling together to form agglomerates of indeterminate size and shape. Sintering, as used by some workers (*20*), provides only a partial answer, since a sintered particle is not homogeneous throughout its body.

The problem of obtaining a suitable model material was solved by dispersing pure carbonyl iron spheres (available in diameters smaller than 3μ) in the form of a dense suspension in air and passing the latter through the reactor at 800°C. The iron particles were rapidly oxidized and melted by the high exothermic heat of combustion. Apparently whenever molten oxides in the dense suspension came into contact with each other, they agglomerated to form larger spheres until they reached the low temperature zone, near the reactor outlet, where they crystallized and solidified. Thus a large assortment of oxide spheres which varied in diameter from 3 to 120μ were collected from the cyclone separator. As will be shown later the great majority of the spheres consisted of compact dense crystals of oxide containing no pores of any size; however occasional large cavities were found to exist in the larger particles which had less time to fuse during oxidation. The electronmicrograph shown in Figure 3 gives an idea of the range of particle sizes studied in this work; a few 3-μ and one 45-μ spheres are seen on top of a larger 100-μ sphere.

The oxide spheres collected in the separators were first fractionated through five screens down to 325 mesh, and four fractions were obtained of mean diameters between 47 and 102 μ. The undersize material from the 325 mesh was separated further by subjecting it to elutriation in a machine which yielded seven size cuts between 3 and 31-μ in diam. The mean arithmetic diameters and respective iron content of the fractions used in the reduction studies are listed below along with the standard deviations from the mean diameter value as calculated for two sizes at random:

Average diameter, μ	% Fe content	Standard deviation from average diameter, μ
5.2	70.8	1.4
10.3	71.9	—
21	71.9	6.0
31	71.8	—
47	72.2	—
63	72.7	—
76	73.1	—
102	73.1	—

(density, 4.7 g./cc.)

Residence-Time Studies

The falling time of the particles through the reactor proper was estimated by calculating the average velocity of the gas stream through the tube and adding to it the average Stokes velocity of the particles in the stream. The accuracy of this calculation was checked experimentally by various visual methods and was found to be quite reliable.

HEAT TRANSFER STUDIES

In order to establish the time-temperature relationship for the oxide particles falling through the reactor it was necessary to determine the rates of heat transfer to the particle by radiation, chemical reaction, and convection. The first and second contributions could be estimated with a certain degree of accuracy from existing theory and by using the reduction-rate Equation (1). However to calculate the rate of convection heat transfer from the gases it was necessary to know the mode of heat transfer between the reactor walls and the gas stream.

The nature of the atomized suspension technique system, which involves high-temperature differentials, low aspect (L/D) ratios, and very low gas Reynolds numbers, is such that the available heat transfer correlations are not directly applicable. Therefore it became necessary to make a brief study of the rate of heat transfer between the walls and a pure gas stream (nitrogen) flowing through the reactor. A complete report of this investigation is presented elsewhere (*21*). The most important result, from the viewpoint of the present study, was the following correlation between Nusselt and Reynolds numbers for diathermanous gases of constant Prandtl number flowing under the conditions of the atomized suspension technique:

$$N_{Nu} = 0.20\ (N_{Re})^{0.71} \qquad (4)$$

By using Equation (4) it was possible to group the three contributions to heat transfer and equate them to the accumulation of heat in a reacting oxide sphere; the differential equation obtained was as follows:

$$dT_p = [3/4r_o^3\,\pi(c_p)_p\,\rho_p]$$
$$[4\pi\,k_g\,r_o(T_g - T_p) + 4\pi\,r_o^2\,\epsilon_p\,\sigma(T_w^4 - T_p^4) + 2\pi\,r_o^2\,\rho_p(\Delta H)k_L (1 - R_x)^{2/3}\,T_p\,e^{-E/RT}]\,d\theta \qquad (5)$$

where T_g was expressed by means of the following differential equation:

$$dT_g = [4h_w(T_w - T_g)/D(3.3 + 4.05 \times 10^{-4}\,T_g)][RT_g/pM + (4.56 \times 10^9\,\rho_p\,r_o^2/G)\,(492/T_g)^{0.695}]\,d\theta \qquad (6)$$

The simultaneous analytical solution of Equations (5) and (6) was impossible since not only T_p and T_g, but also the fractional reduction R_x, were functions of time. However these equations were solved numerically on an IBM-650 digital computer, and the results showed (*21*) that owing to the low endothermic heat involved in reduction the contribution to heat transfer by chemical reaction was not significant in comparison to that of convection. Consequently the temperature difference between gas and suspended oxides was very small for particles of the order of 100 μ and negligible for smaller particles.

The above analytical results were subsequently verified by direct experimental measurements of particle temperatures obtained with the two-wave length radiation pyrometer (*19*). Readings were taken during the reduction of 5- and 31-μ spheres, and the particle temperature was found to agree with ±15°C. with the gas temperature.

This showed that the large coefficients of heat transfer between gas and reactor walls favored rapid heating of the entering cold gas up to the reactor temperature. Therefore by installing an auxiliary furnace and preheating the feed gas up to 500°C. during the reduction tests it was insured that the temperature of the reducing gas approached that of the walls in a very short time interval. Also, since it was established that particle and gas temperatures were approximately equal, it was assumed that the oxide particles were subjected to isothermal reduction during most of their flight in the reactor.

PROCEDURE

The procedure adopted for the reduction studies consisted of heating the reactor walls to a uniform temperature and maintaining a steady supply of hydrogen gas (1.2 to 2.5 std. cu. ft./min.) and dispersed solid particles (1-5 g./min.) to the column. Samples of reduced solids were obtained through the three side ports of the reactor and from the cyclone separator.

The extent of the reduction was estimated by analyzing the samples for per cent iron content and was expressed in terms of the fraction of original oxygen removed by reduction (R_x). No analysis of the gas or material balance were attempted because the hydrogen supply was in large excess of the stoichiometric requirements

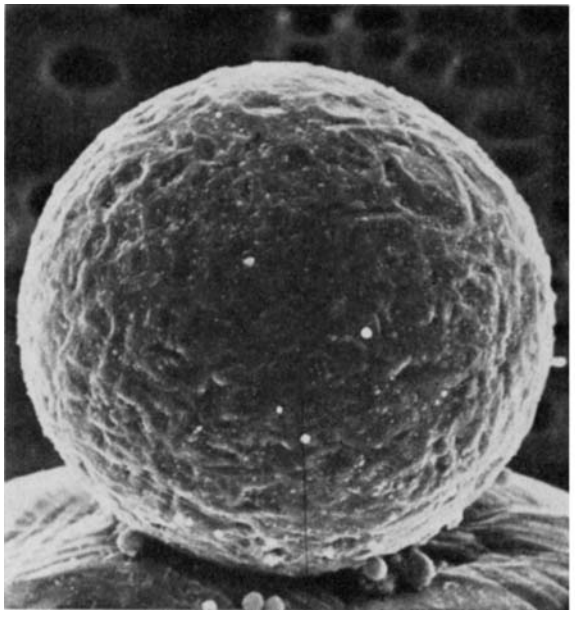

Fig. 3*a*. Iron oxide spheres of various sizes (× 1,700).

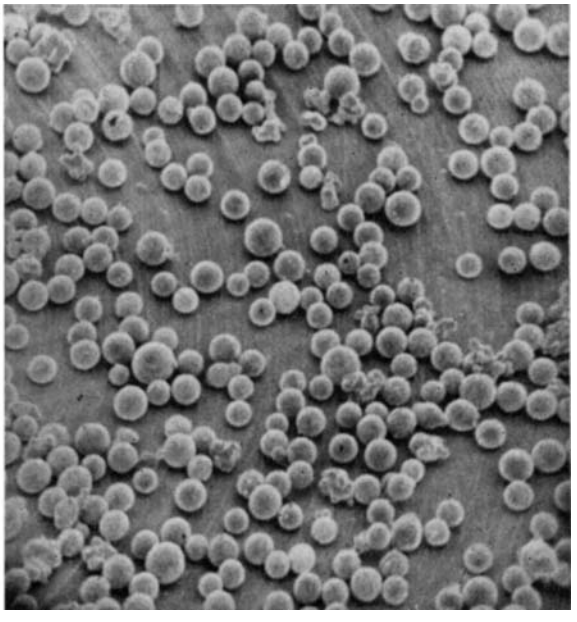

Fig. 3*b*. 20-μ oxide spheres (× 145).

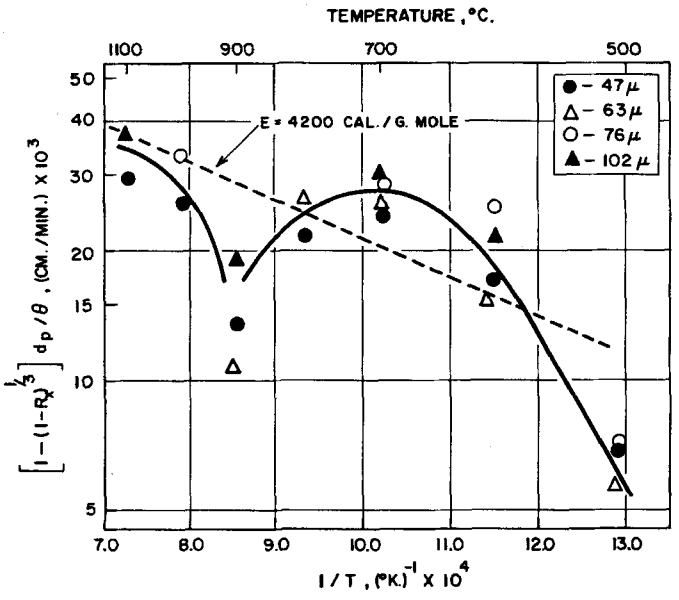

Fig. 4. Effect of temperature on the rate constant of reduction.

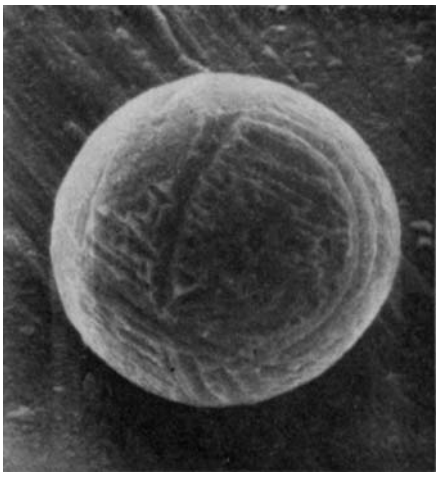

Fig. 5. 20-μ unreduced sphere ($\times$ 2,500).

of the reaction and only a minute fraction of it was actually converted to water vapor.

Other analytical work involved standard X-ray analysis of a small number of samples for identification of oxide phases, and electron micrographic examination of reduced and unreduced particles.

EXPERIMENTAL RESULTS

The reduction studies encompassed eight sizes of oxide spheres between 5 and 102 μ. The particles were reduced at temperatures between 500° and 1,100°C. and in time intervals ranging from 1 to 12 sec. Tabulated operating conditions and experimental results (in the form of fractional reduction accomplished R_x against time of residence in the reactor) can be found in reference 22.

ANALYSIS OF EXPERIMENTAL RESULTS

The reduction data collected indicated that while the larger particles (47 to 102-μ in diam.) obeyed the correlation of Equation (1), the smaller spheres (5 to 31-μ) deviated from this relationship. Accordingly the discussion of the results has been divided into two parts.

47- TO 102-μ SPHERES

The reduction data were plotted in the form of $(1 - R_x)^{1/3}$ against residence time. In agreement with Equation (1) the resulting plots were linear and their slopes m are tabulated in Table 1. In accordance with the same Equation (1) the product md_p (Table 1) should be related only to the temperature of reduction since it actually represents the rate constant for the reaction. Consequently a plot of $\ln(md_p)$ against the reciprocal of the reaction temperature, in accordance with the Arrhenius equation, should yield a straight line of slope proportional to the activation energy of reduction:

$$\ln(md_p) = \ln(md_p)_o - E/RT \quad (7)$$

Actually the resulting plot (Figure 4) was found to be far from linear; the rate constant increased appreciably between 500° and 600°C., the activation energy in this region corresponding roughly to 15,000 cal./g. mole. Between 600° and 700°C. it increased further but at a reduced rate, while in the range of 700° to 900°C., it decreased gradually, reaching its lowest value around 900°C. Finally at reduction temperatures above 900°C. the rate constant started increasing again.

This peculiar behavior of the reduction rate with temperature was not quite unexpected, since a number of previous investigators have reported similar findings. In particular Meyer (23) and Udy and Lorig (24) have found a rapid increase of the rate constant in the low-temperature region and a pronounced drop between 800° and 900°C. The latter authors explained the phenomenon in terms of sintering and crystallization, and the same explanation has been advanced by Tenenbaum and Squarcy (25) and also by Lloyd and Amundson (26); however the latter authors maintain that the inhibiting effect of the higher temperatures becomes only noticeable during the final stages of reduction. The occurrence of sintering, in the usual sense of a phenomenon involving the agglomeration of small particles, was most unlikely in the present work, since the gas-solid system was well dispersed and microscopic examination of the product showed no evidence of particle adherence or agglomeration.

In order to investigate the second possibility of crystallization a series of electron micrographs were obtained on oxide spheres before and after reduction. Some of these photographs are shown in Figures 5 and 6, and a number of others can be found (22). Figure 5 shows the surface of a 20-μ particle before reduction. Some crevasses and surface irregularities are present, but no pores of any kind can be seen. Larger spheres showed surface striations which were probably due to the rapid crystallization of the molten oxide while freely rotating in the gas stream, during the formation of the oxide particles. There is some indication that these striations may represent dislocation planes of the oxide crystals; however a detailed interpretation of this phenomenon is beyond the scope of the present work. Comparison of Figure 5 with the reduced sphere of Figure 6 (obtained at 700°C.) corroborates the main assumption of the mechanism proposed earlier, namely that the removal of oxygen atoms from the oxide crystal results in the appearance of micropores through which the reducing gas can diffuse inwards to the unreduced core. Reduction at 600°C. produced smaller pores, but more numerous per unit area, while the opposite behavior was observed at 800°C. This effect of temperature on the reduced crystals will be discussed later.

Cracking and spalling has been reported by some experimenters during the reduction of oxide lumps. The phenomenon has generally been ascribed to the transformation of the oxide crystal and the resulting weakening of its structure during reduction. It has the effect of accelerating the reaction rate by increasing the surface area exposed to the reducing gas; however very few cracked particles were found in the present work.

The effect of reduction on the internal structure of the particle was investigated further by sectioning re-

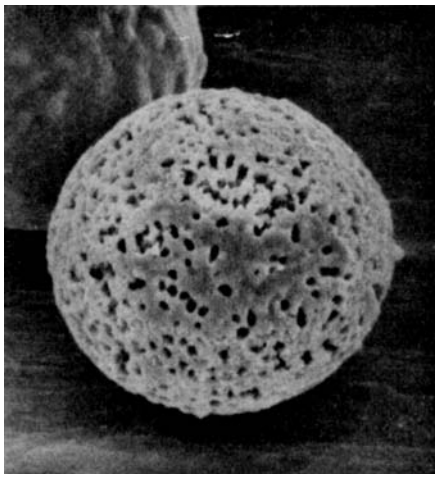

Fig. 6. 20-μ particle reduced at 700°C. (× 2,500).

duced and unreduced spheres and examining them under the electron microscope. Sectioning was effected by embedding the particles in a plastic base, a thin layer of which could be ground and polished after hardening. As may be seen from Figures 7, 8, and 9 the results of this study were highly rewarding. Figure 7 shows that the unreduced spheres consisted of nearly perfect crystals, devoid of any type of microporosity. Occasional isolated imperfections could be noted, especially with the larger spheres, owing to the extremely short time available for formation during their oxidation from iron. Nevertheless it can be safely claimed that on the average the model spheres used in this work consisted of continuous oxide crystals free from the porosity that may be encountered in oxides prepared artificially by sintering of fine particles (*13, 20*).

The effect of reduction on the structure of the spheres is revealed in Figures 8 and 9, which clearly show the body of the reduced particles to be traversed by innumerable channels through which the reducing gas can diffuse to the center of the particle. The difference in pore size and distribution between these two spheres should be noted; the pores were again observed to be larger but fewer at higher temperatures, probably due to crystallization.

The assumption that the reduction proceeds from the outside surface towards the center of the particle, which has already been verified analytically (*1*), is also corroborated by Figure 9, which shows that after partial reduction there exists a reduced outer layer, while the core of the particle has not yet been attacked. The same effect was invariably observed in all the other sectioned spheres which were examined.

In all cases only two solid phases could be identified from the photographs: an outer porous layer of metallic iron, and the unreduced core of the original hematite-magnetite solution. Unfortunately the technical aspects of electron microscopy did not allow phase identification by staining techniques (*7, 27*). Similarly X-ray methods (*9, 26*) could not be applied successfully owing to the difficulty of assuring that the powdered sample consisted of particles of equal size, subjected to the same degree of reduction. However it seems quite doubtful that in the short reaction time available a solid state reaction between iron and magnetite (of the type responsible for the appearance of intermediary oxides) could occur to an appreciable extent. The same should be true of the diffusion of iron atoms through oxides, which has been observed by some experimenters in connection with the reduction of oxide lumps over long time intervals (*28, 29, 30, 31, 32*).

The microscopic investigation also shed some light on the effect of temperature on the rate of reduction. Thus by comparing a sphere reduced at 800°C. with one reduced at 600°C. it would appear that a regrouping of the reduced iron atoms has occurred at the higher temperature, thereby resulting in fewer holes of larger diameter. The same phenomenon is much more pronounced in the case of reduction at 900°C., as shown by Figure 10. This electron micrograph shows that a definite crystallization must have taken place and offers a possible explanation for the drop in reaction rate observed in this temperature range. Apparently the removal of oxygen atoms from the oxide lattice by reduction leaves a skeleton lattice of iron atoms which, as the reaction temperature rises, crystallizes to the thermodynamically more stable iron crystal lattice. The density of the latter is nearly twice that of the original oxide, but since the outside dimensions of the particle do not change appreciably, crystallization results in the appearance of dense cubic iron crystals and corresponding isolated large cavities. The phenomenon apparently starts at low temperatures but increases noticeably over 700°C.

Fig. 7. View of sectioned 20-μ unreduced particle (× 3,800, at 45 deg. to surface).

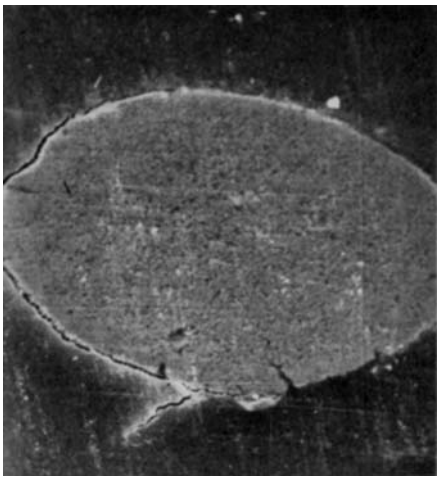

Fig. 8. Section of 76-μ particle totally reduced at 600°C. (× 1,600).

The appearance of cubic crystals during reduction at 900°C., and the corresponding drop in reduction rate may also be associated with the transformation of alpha iron to the gamma crystal, which reportedly takes place at 906°C.; at this temperature the crystal lattice changes from body-centered cubic (two atoms per unit cell) to face-centered cubic (four atoms per unit cell). The free energy associated with this transformation may explain the rapid increase in crystallization in this temperature range.

It should be noted that the cavities ensuing from the reduction at 900°C. are of rectangular cross section owing to the fact that they are bounded by crystals of this shape. During reduction at 1,000°C. the same type of rectangular passages can be observed on the surface of the particle, although the crystal formation is not as well defined as at 900°C. These passages were found to be formed preferentially along the striation lines which were mentioned earlier. Finally, at 1,100°C. (Figure 11), neither the crystals nor the free passages seem to have a regular formation and the surface of the particle becomes amorphous, as if the fusion point of the metal were being approached.

The phenomenon of crystallization can explain the peculiar behavior of the reaction rate with temperature, since the temperature not only in-

Table 1. Calculated Constants Moving Particles (47- to 102-μ)

Particle diameter, μ	Temp., °C.	$1/T$, (°K.)$^{-1} \times 10^4$	m, min.$^{-1}$	md_v, (cm./min.) $\times 10^3$	$me^{E/RT}$, min.$^{-1}$
47	500	12.9	1.55	7.29	24.2
47	600	11.5	3.66	17.2	41.7
47	700	10.2	5.04	23.7	44.4
47	900	8.53	2.87	13.5	17.4
47	1,000	7.85	5.52	25.9	29.0
47	1,100	7.28	6.18	29.1	28.9
63	500	12.9	0.92	5.79	14.4
63	600	11.5	2.45	15.4	27.9
63	700	10.2	4.08	25.7	35.8
63	900	8.53	1.71	10.8	10.3
76	500	12.9	0.92	6.99	14.4
76	600	11.5	3.32	25.2	37.8
76	700	10.2	3.80	28.9	33.4
76	800	9.32	2.84	21.6	20.4
76	1,000	7.85	4.38	33.3	23.0
102	600	11.5	2.10	21.4	24.0
102	700	10.2	2.88	29.4	25.4
102	800	9.32	2.58	26.3	18.5
102	900	8.53	1.86	19.0	11.3
102	1,100	7.28	3.66	37.3	17.1

creases the rate of the interface reaction but also promotes the rate of crystallization; the latter, in turn, inhibits the overall reduction of the oxide by reforming the reduced layer and effectively eliminating some of the passages open to the reducing gas. The over-all porosity does not change during crystallization, since its effect is to produce fewer channels of larger dimensions. However increasing the size of the channels has no effect on the gaseous diffusional resistance since the latter, as mentioned earlier, is apparently negligibly small even in the case of the small channels formed during reduction at lower temperatures. On the other hand fewer channels per surface area of the particle mean that some sections of the interface between reduced and unreduced phases may be cut off from access to the reducing gas and therefore may be bypassed by the advancing reaction front. This would of course result in a lowering of the calculated overall reduction rate, especially during the final reduction stages (*25, 26*).

Although crystallization lowers the reaction rate, it does not necessarily alter the mechanism of the reduction which is still controlled by the interface reaction. The lowering of the rate is due solely to the decrease in interface area accessible to the reducing gas. The mechanism of reduction may only change during the final stage of reduction when pockets of oxide may be cut off from the gas by a shield of crystallized iron; in this case further reduction can take place only by solid state diffusion of iron atoms (*7, 28, 29, 30, 31, 32*).

The evidence presented above supports further the contention of the authors that it is impossible to define a pure chemical activation energy for the reduction of iron oxides above 500°C. On the other hand a temperature coefficient may be selected which best represents the combined effect of temperature on the rate of reduction over the whole range. As mentioned earlier, such an average value was estimated at 4,200 cal./g.-mole (*1*). A dotted line corresponding to this value is shown superimposed on Figure 4. This line does not represent adequately the reduction data at 500°C. since at that temperature crystallization seems to have taken no effect and the change with temperature is still quite rapid. The data obtained at 900°C. also deviate appreciably from the temperature-coefficient of 4,200 cal./g.-mole, while the rest of the data are represented adequately by this line.

Although the scatter of the reduction data from the dotted line may seem considerable, it should be remembered that this line was derived originally for particles a thousandfold larger than the ones used in the present investigation. The fact that it can also correlate the latter to a certain extent indicates that the value of 4,200 cal./g.-mole is probably as satisfactory an approximation to the temperature coefficient as can be made in this complex situation.

With this value of temperature coefficient the values of the reaction rate for the particles ranging from 47 to 102-μ in size were calculated (Table 1) and (with the exception of the 500°C. data) were plotted on the correlation graph shown in Figure 12, which includes the data previously derived in reference *1*. In spite of the mild scatter it is apparent from this plot that the reduction data for conveyed particles in the range of 47 to 102-μ can be correlated quite satis-

Fig. 9. Section of 76-μ sphere reduced outer layer and unreduced core (700°C., × 9,200).

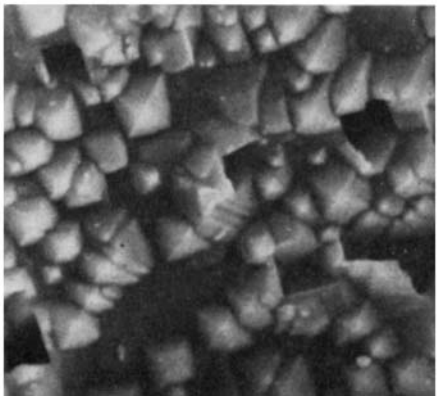

Fig. 10. Surface of 46-μ particle reduced at 900°C. (× 8,800).

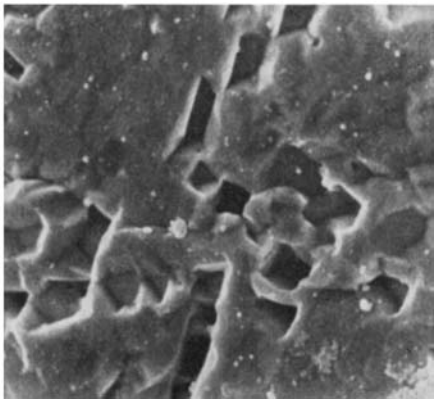

Fig. 11. Surface of 102-μ particle reduced at 1,100°C. (× 4,600).

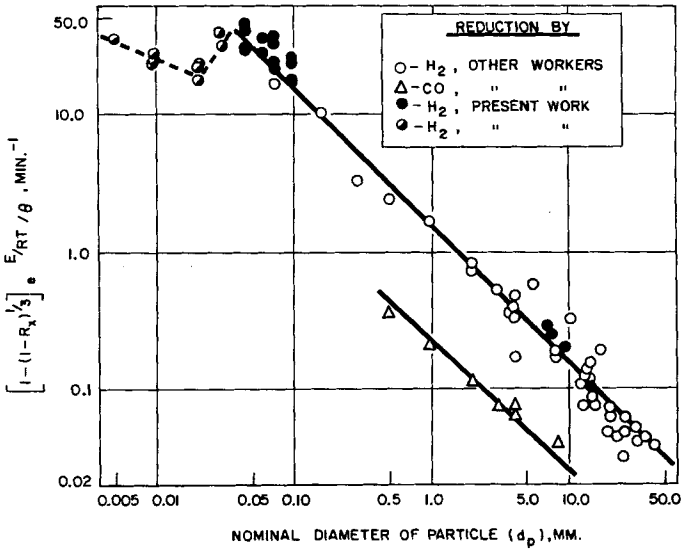

Fig. 12. Correlation of reaction constants.

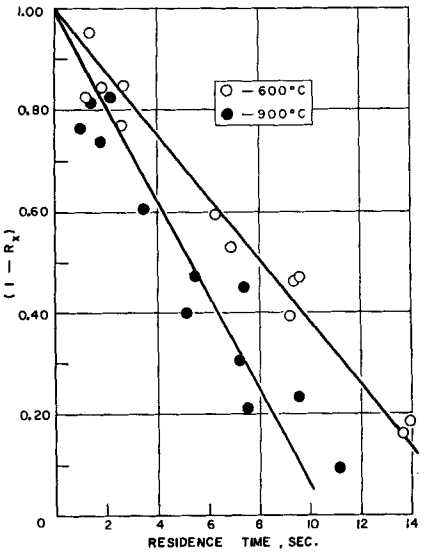

Fig. 13. Reduction of 21-μ particles.

factorily by means of Equation (1), which is represented by the upper solid line.

5.2- TO 31-μ SPHERES

The reduction data for these particles were first plotted in the form of $(1 - R_x)^{1/3}$ against residence time. Although the resulting plots were no longer linear [as would have been expected if Equation (1) still applied], straight lines could be drawn through the experimental points as an approximation and the resulting slopes were plotted on the correlation of Figure 12 (black semicircles). As may be seen from this plot the reaction rates for the 31-μ particles fell slightly below the correlation line, while those for the 21-μ spheres were appreciably lower than would be predicted by Equation (1). For the 10- and 5-μ spheres the reaction rate again increased with a decreasing diameter, but the resulting line was well below the established correlation.

This abrupt deviation from Equation (1) must be ascribed to a change in the controlling mechanism at a critical value of the particle diameter. The first possibility that suggests itself is that of a large increase in the diffusional resistance through the boundary layer. The calculations which were carried out to test this possibility showed immediately that it was untenable. It is however instructive to discuss these results briefly.

At low rates of mass transfer the mass transfer coefficient k_g may be predicted from the Ranz and Marshall correlation (34) with good accuracy:

$$k_g = (2D_v/RTd_p)\,[1 + 0.30(N_{Re})^{1/2}\,(N_{Sc})^{1/3}] \quad (8)$$

For the present case the particle Reynolds numbers were very low (from 0 to 0.15), and Equation (8) was simplified to

$$k_g = 2D_v/RTd_p \quad (9)$$

Theoretical values of k_g calculated from this expression ranged from 1.09 for the 5.2-μ particles to 0.230 for the 31-μ particles. These values were then compared with the experimental k_g's calculated from the rate of water vapor evolution by means of the following expression, with the assumption that the partial pressure of the water vapor at the particle surface was the equilibrium value dictated by the reaction:

$$dN/d\theta = k_g A(p_e - p) \quad (10)$$

The number of pound-moles of water diffusing per unit time ($dN/d\theta$) may also be expressed in terms of the fractional reduction R_x as follows:

$$dR_x/d\theta = 1.5k_g(p_e - p)/\rho_p a d_p \quad (11)$$

In the present case p (the pressure of water vapor in the gas stream) may be assumed to be negligible.

The reduction data for particles between 5 and 31-μ were plotted in the form of $(1 - R_x)$ vs. time, a typical plot of which is shown in Figure 13. From the slopes of these lines the experimental values of k_g were calculated by means of Equation (11). These were smaller by a factor of 10^4 to 10^5 than the calculated values. Thus the experimental rate is very much smaller than the diffusional rate that would be expected for particles of these sizes, and it must be concluded that reduction in the fine-particle range is not controlled by diffusion.

Another possible explanation for the different behavior of very fine particles may be associated with certain surface forces, the existence of which has been known for a long time. This phenomenon, which was first studied by Hertz (35) and later by Knudsen (36), Langmuir (37), and others, arises from the fact that gas molecules generated at a crystalline surface must first diffuse over the surface before they can leave the latter at certain well-defined points. A good review of this subject can be found in a recent paper by Sherwood and Cooke (38). These forces are exceedingly small and are normally observed only at very low pressures. They may however assume a controlling importance for very small particles, in which case they give rise to the following rate equation:

$$-dN/d\theta = \alpha A\sqrt{Mg_c/2\pi RT}\,(p_e - p) \quad (12)$$

where the value of α (called the *accommodation coefficient*) represents the rate constant of the process and has been reported to vary somewhat with the curvature of the particle.

The assumption may therefore be made that this resistance is quite less than that of chemical reaction for the range of particles included in the correlation of Equation (1) and only becomes appreciable for the very fine particles below 40 μ in diameter. Its increase in this range may be due to the rapid change in curvature.

It is felt that the reduction data for only three particle sizes (since the 31-μ spheres seem to lie in the transition range) are not sufficient to support the above hypothesis nor to permit the formulation of the new mechanism which is apparently controlling the reduction of the very fine spheres. Nevertheless the data have been valuable in establishing the lower limit of the correlation developed earlier [Equation (1)] and in indicating the trend of reduction rates that should be expected for oxide particles below 325 mesh in size.

CONCLUSIONS

The data obtained during reduction of the larger moving particles confirmed further the validity of the rate theory (*1*). On the other hand, for particles below 31 μ in diam., the experimental results deviated from the established correlation. It is believed that in this range a transition takes place in the controlling factor from chemical resistance to a two-dimensional surface phenomenon. However the data in this size range are too limited to allow the formulation of the new controlling mechanism.

The evidence supplied by the electron microscope studies lends strong support to the theory that reduction is initiated at the surface of the particle and proceeds inwards by means of diffusion of the reducing gas through the micropores of the reduced layer.

The effect of temperature was studied by means of reduction data and also by microscopic examination of the reduced particles. It was concluded that up to 600°C. the temperature has a strong effect on the rate of reduction, as would be expected for a purely chemical reaction. Above 600°C. the rate of crystallization of the reduced layer becomes significant and inhibits the access of reducing gas to parts of the unreduced core.

Consequently the apparent effect of temperature on reduction is the resultant of the combined phenomena of chemical reaction and crystallization. The influence of the latter becomes so pronounced at 800° to 900°C. that an increase in temperature in this range actually lowers the reduction rate appreciably. It is quite probable that the phase transformation from alpha to gamma iron, which takes place at 906°C., accelerates the rate of crystallization in this region.

At temperatures higher than 900°C. the rate again increases with temperature. In effect these results affirmed the necessity of defining an average temperature coefficient rather than an activation energy in the true chemical sense.

NOTATION

a = lb. moles of water produced on total reduction of 1 lb. of oxide

A = surface area of particle, sq. ft.

c_e, c = concentration of water vapor at equilibrium and in the bulk stream, respectively, lb. moles/cu. ft.

c_p = heat capacity of gas, B.t.u./lb. °R.

$(c_p)_p$ = heat capacity of solid particles, B.t.u./lb. °R.

$dN/d\theta$ = lb. moles of water vapor produced/sec.

D = reactor diameter, ft.

d_p = particle diameter, ft. [cm. in Equations (1), (2), and (3)]

D_v = diffusivity of water vapor in hydrogen, sq. ft./hr.

E = temperature coefficient of reduction, cal./g. mole (for hydrogen reduction, E: 4,200)

G = mass velocity of gas, lb./sq. ft. hr.

g_c = dimensional constant, 32.2 poundals/lb.-force

h_w = heat transfer coefficient at reactor wall, B.t.u./hr. sq. ft. °R.

k_g = mass transfer coefficient, lb. moles/hr. sq. ft. (lb./sq. ft.)

k_L = linear rate constant for the reduction of iron oxides (for hydrogen reduction, k_L = 0.150 cm./min.)

m = $\dfrac{\Delta(1-R_x)^{1/3}}{\Delta\theta}$, min.$^{-1}$

M = molecular weight of water, lb./lb. mole

p_e, p = partial pressure of water vapor at equilibrium and in the bulk stream, respectively, lb./sq. ft.

R = universal constant, 1.98 cal./(g. mole × °K.) or (B.t.u./lb. mole × °R.)

R_x = fractional reduction (fraction of total oxygen removed)

r_o = radius of spherical particle, ft.

T = reduction temperature, °K. (or °R.)

T_g = gas temperature, °R.

T_p = particle temperature, °R.

T_w = reactor wall temperature, °R.

V_R = relative velocity between particle and gas, ft./sec.

Greek Letters

α = accommodation coefficient, dimensionless

ΔH = heat of reaction, (for reduction of iron oxide = 285 B.t.u./lb.)

ϵ_p = emissivity of particle, dimensionless

μ = viscosity of gas, lb./ft. sec.

ρ_p = oxide density, lb./cu. ft.

ρ = gas density, lb./cu. ft.

σ = Stefan-Boltzmann constant, 0.173×10^{-8} B.t.u./(hr.)(sq. ft.)(°R.)^4

θ = reaction time, sec. [min. in Equations (1), (2), and (3)]

Dimensionless Groups

N_{Nu} = Nusselt number

N_{Re} = Reynolds number

N_{Sc} = Schmidt number

LITERATURE CITED

1. Themelis, N. J., and W. H. Gauvin, *Trans. Am. Inst. Mining, Met., Petrol. Engrs.*, to be published.
2. Lewis, J. R., *ibid.*, **172**, 27 (1947).
3. Melcher, G., and E. V. Cajado, *Bol. assoc. brasil. metais*, **5**, 341 (1949).
4. Bogdandy, L. V., and W. Janke, *Z. Electrochem.*, **61**, 1146 (1957).
5. Stalhane, B., and T. Malmberg, *Jernkontorets Ann.*, **114**, 1 (1930).
6. *Ibid.*, p. 609. (H. Brutcher translation 1870).
7. Edstrom, J. O., *J. Iron Steel Inst.*, **175**, 289 (1953).
8. ———, *Jernkontorets Ann.*, **140**, 116 (1956). (H. Brutcher translation 3886.)
9. Lloyd, W. A., Ph.D. thesis, Univ. Minnesota, Minneapolis, Minnesota (1954). (Univ. Microfilms, Ann Arbor, Mich. 56-1449.)
10. Wiberg, M., *Jernkontorets Ann.*, **124**, 179 (1940).
11. Rostovtsev, S. T., and A. P. Em, *Doklady Akad. Nauk S.S.S.R.*, **93**, 131 (1953).
12. Joseph, T. L., *Trans. Am. Inst. Mining, Met., Petrol. Engrs.*, **120**, 72 (1936).
13. McKewan, W. M., *ibid.*, **218**, 2 (1960).
14. Ezz, S. Y. M., and R. Wild, *J. Iron Steel Inst.*, **194**, 211 (1960).
15. Gauvin, W. H., *Chem. in Can.*, **7**, 48-56 (1955).
16. ———, *Tappi*, **40**, No. 11, pp. 866-872 (1957).
17. Lee, G., N. J. Themelis, and W. H. Gauvin, *ibid.*, **41**, 312 (1958).
18. Mathur, K. B., and P. E. Gishler, *A.I.Ch.E. Journal*, **1**, 157 (1955).
19. Themelis, N. J., and W. H. Gauvin, *Can. J. Chem. Eng.*, to be published.
20. Dalla Lana, I. G., and N. R. Amundson, *Ind. Eng. Chem.*, **53**, 22 (1961).
21. Themelis, N. J., and W. H. Gauvin, *Can. J. Chem. Eng.*, to be published.
22. Themelis, N. J., Ph.D. thesis, McGill University, Montreal, Quebec, Canada (1961).
23. Meyer, H. H., *Kaiser-Wilhelm Inst., Eisenforsch*, **10**, 72 (1928).
24. Udy, M. C., and C. H. Lorig, *Trans. Am. Inst. Mining, Met., Petrol. Engrs.*, **154**, 162 (1943).
25. Tenenbaum, M., and C. M. Squarcy, Reprint of paper presented Am. Iron and Steel Inst., New York (May, 1951).
26. Lloyd, W. A., and N. R. Amundson, *Ind. Eng. Chem.*, **53**, 19 (1961).
27. Bitsianes, G., and T. L. Joseph, *Trans. Am. Inst. Mining, Met., Petrol. Engrs.*, **200**, 150 (1954).
28. Wagner, C., *ibid.*, **194**, 214 (1952).
29. Moskvicheva, A. G., and C. I. Chufarov, *Doklady Akad. Nauk S.S.S.R.*, **105**, 510 (1955).
30. Richardson, F. D., and E. Dancy, *Discussions Faraday Soc.*, No. 4, p. 229 (1948).
31. Gellner, O. H., and F. D. Richardson, *Nature*, **168**, 23 (1951).
32. Himmel, L., R. F. Mehl, and C. E. Birchenall, *Trans. Am. Inst. Mining, Met., Petrol. Engrs.*, **197**, 827 (1953).
33. Kawasaki, Edward, Jack Sanscrainte, and T. J. Walsh, *A.I.Ch.E. Journal*, **8**, No. 1, p. 48 (1962).
34. Ranz, W. E., and W. R. Marshall, Jr., *Chem. Eng. Progr.*, **48**, 141, 173 (1952).
35. Hertz, H., *Ann. Phys.*, **17**, 177 (1882).
36. Knudsen, M., *ibid.*, **47**, 697 (1915).
37. Langmuir, I., *Phys. Rev.*, **2**, 329 (1913).
38. Sherwood, T. K., and N. E. Cooke, *A.I.Ch.E. Journal*, 3, 37 (1957).

Manuscript received September 12, 1961; revision received January 5, 1962; paper accepted January 8, 1962. Paper presented at A.I.Ch.E. New York meeting.